Journal of Experimental Botany, Vol. 00, No. 0 pp. 1–13, 2026
https://doi.org/10.1093/jxb/erag110 Advance Access Publication 27 February 2026

RESEARCH PAPER

Leaf width expansion and biomass allocation, rather than photosynthetic rate, drive early vigor in newly developed rice lines

Ya Zhang, Xianke Yang, Xiaoxia Ling, Kehui Cui, Jianliang Huang, Shaobing Peng, and Dongliang Xiong*

National Key Laboratory of Crop Genetic Improvement, Hubei Hongshan Laboratory, MARA Key Laboratory of Crop Ecophysiology and Farming System in the Middle Reaches of the Yangtze River, Huazhong Agricultural University, Wuhan, Hubei 430070, China

* Correspondence: dlxiong@mail.hzau.edu.cn

Received 22 September 2025; Accepted 24 February 2026

Editor: Robert Sharwood, Western Sydney University, Australia

Abstract

Early seedling vigor is a key determinant of rapid canopy establishment and early biomass production in rice, yet its physiological and morphological drivers remain incompletely understood. Rapid growth is often assumed to result from enhanced leaf-level photosynthetic capacity, but this assumption has rarely been tested explicitly. Here, we examined growth dynamics, biomass allocation, leaf morphology, and photosynthetic traits in newly developed rice lines exhibiting strong early vigor and compared them with the elite cultivar HHZ. The new lines accumulated biomass more rapidly than HHZ and exhibited non-exponential growth patterns, with higher absolute and relative growth rates. Despite lower leaf photosynthetic rates and lower leaf nitrogen content, the new lines showed significantly greater early biomass accumulation and larger canopy leaf area than HHZ. Canopy expansion was driven mainly by increased leaf width, rather than leaf length or leaf number per tiller, together with a greater allocation of biomass to leaves relative to roots during early growth. These results demonstrate that rapid early growth can be achieved through a canopy expansion strategy that prioritizes leaf morphological development and biomass allocation over photosynthetic efficiency per unit leaf area. This observation entails clear trade-offs, including nitrogen dilution and reduced photosynthetic biochemical capacity, yet it results in greater whole-plant biomass accumulation during early establishment. Our findings challenge the conventional assumption that early vigor is necessarily associated with higher leaf photosynthesis and highlight alternative physiological pathways for improving early growth and competitiveness in rice.

Keywords: Biomass allocation, early vigor, genotype, photosynthesis, relative growth rate.

Introduction

Rapid early crop growth, often referred to as early seedling vigor, describes the ability of crops to grow promptly before their canopy closes (Cairns *et al.*, 2009; Rebolledo *et al.*, 2012; Zhao *et al.*, 2019). Early vigor is crucial because it allows for quick canopy establishment and efficient acquisition of essential resources such as light, water, and nutrients, thereby improving resource use efficiency and enhancing the competitiveness of crops against weeds (Duan *et al.*, 2016; Aharon *et al.*, 2021;

Xiong, 2024). Additionally, rapid early growth is particularly important in crop rotation systems, as continuous planting often requires shorter crop growth periods to fit multiple rounds of crops, and the rapid early growth can compensate for the growth loss caused by the shortened periods (Rebolledo *et al.*, 2012).

Over the past decade, our research group has developed several new rice lines using the pedigree method that exhibit rapid biomass accumulation during the vegetative stage (Pan *et al.*, 2023). However, the mechanisms underlying this rapid growth remain unclear. To quantitatively assess growth, the absolute growth rate (AGR) and the relative growth rate (RGR) are widely used to measure biomass accumulation (Hilty *et al.*, 2021). AGR quantifies the increase in biomass over a specific period, while RGR provides a measure of biomass increase relative to the initial biomass (Paine *et al.*, 2012). RGR is particularly insightful because it accounts for the initial size of the organism, making it a more standardized growth metric compared with AGR (Blackman, 1919; Pommerening and Muszta, 2016; Lamont *et al.*, 2023).

Typically, RGR at the early growth stages of a plant is calculated using an exponential model that assumes a constant rate throughout the period, though this assumption is rarely valid (Rebolledo *et al.*, 2012, 2013; Fletcher *et al.*, 2022). Indeed, many studies have suggested that the exponential approach is oversimplified and that RGR usually decreases during certain developmental stages due to factors such as the accumulation of non-photosynthetic biomass (e.g. stems, sheaths, and roots), leaf self-shading, and reduced local soil nutrient concentrations (Tessmer *et al.*, 2013; Hilty *et al.*, 2021). To overcome the limitations of the exponential model, the power-law model is an alternative that can more accurately describe how RGR evolves over time and with increasing biomass (Paine *et al.*, 2012), depending on the value of the exponent β (Supplementary Fig. S1). In this model, a β value of 0 signifies a linear relationship. If β is between 0 and 1, the RGR progressively decreases. A β of 1 indicates an exponential model where the RGR remains constant. When β exceeds 1, the RGR increases as biomass increases. Therefore, the first objective of this study is to examine the patterns of biomass accumulation and the dynamics of the power-law growth model for AGR and RGR in newly developed rice lines during their initial growth stages.

Early growth rates in plants are influenced by the allocation of biomass among different plant organs (Shipley and Meziane, 2002; Poorter *et al.*, 2012; Weraduwage *et al.*, 2015). During initial growth stages, limited carbon resources mean that allocating more carbon to leaf development enhances light capture but restricts the carbon available for root development, which is vital for water and nutrient absorption (van den Boogaard *et al.*, 1996; Liao *et al.*, 2004; Shiraiwa *et al.*, 2006). In flooded rice systems, however, soils are typically nutrient rich during early development due to basal fertilizer application, and seedlings are small, resulting in minimal competition for below-ground resources (Gu and Yang, 2022). Under these conditions, relatively small root systems can support early growth, potentially allowing plants to prioritize carbon allocation to leaf development.

As a result, rapid early growth can be achieved through two contrasting strategies (Xiong, 2024). One strategy emphasizes higher photosynthetic efficiency per unit leaf area through greater investment in photosynthetic machinery and supporting root systems. The alternative strategy prioritizes rapid canopy expansion through increased biomass allocation to leaves and accelerated leaf morphological development. Rapid morphological expansion of leaves may dilute nitrogen concentration per unit leaf area and limit photosynthetic capacity, whereas greater investment in photosynthetic machinery and roots may restrict early canopy expansion and slow early biomass accumulation (Yao *et al.*, 2014; He *et al.*, 2022).

Leaf morphological traits therefore play a central role in shaping early canopy development. In wheat, research by Rebetzke *et al.* (2007) identified the length of the coleoptile and the width of the second leaf as heritable traits linked to early vigor. This is further supported by Zhang *et al.* (2015), who found that broader leaves in wheat led to larger early leaf areas and increased biomass. These studies indicate that selecting wider leaves could significantly boost early growth vigor in wheat. However, studies on the relationship between leaf traits and early growth rate in rice are rare. The investigation in rice found that there is only a weak correlation between the length of the seventh leaf and the RGR, and no correlation with the width of the seventh leaf (Rebolledo *et al.*, 2012). By the time the seventh leaf is fully expanded, however, the plant already has a large canopy, indicating that the influence of the morphology of a single leaf on growth rate might be minimal due to the presence of other leaves. Early vigor, therefore, may emerge from coordinated variation in leaf morphology, biomass allocation, and leaf physiological properties. In addition to total leaf area, traits such as leaf width and length, leaf mass per area (LMA), and leaf nitrogen content determine how rapidly canopy structure is formed and how efficiently carbon is assimilated per unit leaf area (Xiong and Flexas, 2018; Xiong, 2024). These traits provide mechanistic links between canopy development, photosynthetic performance, and whole-plant growth. A comprehensive understanding of early vigor thus requires integrating morphological and nutrient-related leaf traits with growth analysis.

Based on this conceptual framework, we tested four specific hypotheses relating to the early vigor of our newly developed lines. (i) Rapid early growth in the newly developed rice lines is driven primarily by increased allocation of biomass to leaves and accelerated expansion of canopy leaf area, rather than by higher photosynthetic capacity at the leaf level. (ii) The larger leaf area observed in the new lines arises mainly from morphological expansion of individual leaves, particularly through increased leaf width rather than increased leaf number or leaf length. (iii) Rapid leaf area expansion is associated with

physiological trade-offs, including lower leaf nitrogen concentration, altered LMA, reduced photosynthetic biochemical capacity, and lower CO_2 diffusion conductance. (iv) Early vigor represents a whole-plant strategy that prioritizes canopy development and early biomass productivity over photosynthetic efficiency per unit leaf area, thereby resulting in higher early biomass accumulation despite lower rates of leaf-level photosynthesis, which is expected to enhance crop competitiveness and productivity in direct-seeded and short-season rice systems.

Materials and methods

Plant materials

Three newly developed rice lines—CPPC15, CPPC18, and CPPC52—along with Huanghuazhan (HHZ), a widely used local cultivar and currently the most widely used genotype for direct seeding in the region, were used in this study. For these four genotypes, seeds harvested from the same growth season were used. The seed weights and seedling development during the first 5 d after sowing of each genotype are shown in Fig. 1. CPPC15, CPPC18, and CPPC52 were selected from a genetically diverse composite cross involving three parent lines, Zaoxian 615, Xiangzaoxian 6, and Jiazao 5. These lines were developed to improve grain yield in rice-based rotational cropping systems, in particular for the direct-seeding double-season rice system recently practised in the middle reaches of the Yangtze River. The individual selections based on above-ground biomass accumulation and grain yield began in 2014 under field conditions (Pan *et al.*, 2023), and seeds harvested from self-pollinated F_8 plants under field conditions were used in this study. Detailed haplotype composition and genome-wide introgression patterns were not determined in this study and will require future genetic analysis.

Both pot and field experiments were conducted at the rice field station on the campus of Huazhong Agricultural University (114.37 E, 30.48 N) in July and August 2023. The climate information including air temperature, relative humidity, and photosynthetic photon flux density (PPFD) over the experimental period are provided in Supplementary Fig. S2. A completely randomized block design with four plot replicates for each genotype was adopted for field experiments. To minimize the influence of the seed germination process on our investigation, seeds with emerged coleorhiza were uniformly sown using a matrix localization method at a density of 50 seeds m^{-2}. For each replicate, the plot size was 6 m^2. Under pot conditions, the coleorhiza emerged seeds were directly sown in 13 liter cylindrical pots containing 10 kg of dry soil at a density of 12 seeds per pot, and the seeds were uniformly distributed using a net. The depth of the pot is 25 cm, and the diameter is 24 cm. In the field, 18 g of nitrogen (N), 4.0 g of phosphorus (P), and 10.0 g of potassium (K) were applied per plot, while 10.0 g of compound fertilizer ($N:P_2O_5:K_2O$=17:17:17%; Sanning Chemical Co., Ltd, Yichang, China) was pre-mixed into the dry soil of each pot. During the experiment, diseases, pests, and weeds were meticulously managed. Potted plants were grown outdoors. As the canopy of the newly developed lines closed ~40 d after sowing under both pot and field conditions, we investigated the growth of the plants over the first 43 d only.

Growth performance

To monitor temporal growth dynamics, we regularly sampled plants to assess the growth of each organ. In the field, for each plot, four plants were harvested on 16, 26, and 36 d after sowing. For potted plants, harvesting occurred at 11, 16, 21, 26, 31, 36, and 43 d after sowing, with four pots per genotype collected at each time point. After measuring plant height, tillering, and the number of fully developed leaves, the entire plant, including the root system, was washed free of soil. In the lab, samples were separated into roots, stems, and leaves, and green leaf area was measured using a leaf area meter (LI-3000, LI-COR Inc., Lincoln, NE, USA). Samples were then dried in an oven at 80 °C for 2–3 d and weighed using a Mettler Toledo balance (model MS205DU, Mettler-Toledo GmbH, Greifensee, Switzerland). In addition, the length and width of the first five true leaves were measured once the leaves were fully expanded.

Gas exchange

Since the plants were too small, gas exchange could not be estimated for the first five leaves. Gas exchange along with chlorophyll fluorescence were measured on the fully developed sixth leaves of potted plants using a LI-6800 portable photosynthesis system (LI-COR), between 16 d and 20 d after sowing. To reduce the impact of environmental variations, the pots were placed in an controlled-environment room 1 d before the measurements. The room maintained a temperature of 28 °C during the day and 24 °C at night, 65% relative humidity, and a light intensity of ~400 μmol m^{-2} s^{-1} on the leaf surface.

Initially, the light response curves were measured for each genotype. For the light response curve, the leaf temperature inside the gas exchange chamber was set to 28 °C, the reference CO_2 concentration was 400 μmol mol^{-1}, and relative air humidity was 65%. Leaves were acclimated to a PPFD of 1500 μmol m^{-2} s^{-1} until the photosynthetic rate stabilized, which typically took 20–40 min. The auto-progression of the light response curve was then conducted by adjusting the PPFD to 2000, 1500, 1200, 1000, 800, 600, 400, 200, 150, 100, 50, and 0 μmol m^{-2} s^{-1} in series at intervals of 60–90 ss. After estimating the light response curves, the CO_2 response curves for each genotype were measured under the same environmental conditions. As the PPFD values at 75% saturation of photosynthesis estimated from light response curve for all the genotypes were ~1000 μmol m^{-2} s^{-1} (see the Results), the PPFD for the CO_2 response curve was set to 1500 μmol m^{-2} s^{-1}. Once the photosynthetic rate stabilized in the gas exchange chamber with 400 μmol mol^{-1} CO_2 concentration and the PPFD at 1500 μmol m^{-2} s^{-1}, determination of the CO_2 response was conducted by adjusting the CO_2 concentrations to 400, 300, 200, 100, 50, 400, 600, 800, 1000, 1200, 1500, and 2000 μmol mol^{-1} in series at intervals of 90–120 s. For each gas exchange measurement, values of steady-state fluorescence (F_s) and maximum fluorescence in light conditions (F_m') were recorded.

The light response curve was fitted using the non-rectangular hyperbola-based model:

$$P_n = \frac{\Phi \times PPFD + A_{gmax} - \sqrt{(\Phi \times PPFD + A_{gmax})^2 - 4\theta \times \Phi \times PPFD \times A_{gmax}}}{2\theta} - R_n$$

P_n is the net photosynthetic rate, Φ is the quantum yield representing the amount of CO_2 fixed per unit of light absorbed, A_{gmax} is the maximum gross photosynthetic rate, θ is the convexity factor, and R_n is dark respiration. The model was fitted to the data using the orthogonal non-linear least-squares regression (ONLS) model in the R program.

The CO_2 response curves were fitted using the R package 'plantecophys', and the A–C_i-based maximum carboxylation rate (V_{cmax}) and maximum electron transport rate (J_{max}) were extracted. The first measurement on each CO_2 response curve was extracted and analyzed as the steady-state gas exchange measurement. The actual photochemical efficiency of PSII (Φ_{PSII}) and the electron transport rate (ETR) were calculated as follows:

$$\Phi_{PSII} = \frac{F_m' - F_s}{F_m'}$$

$$ETR = \Phi_{PSII} \times PPFD \times \alpha\beta$$

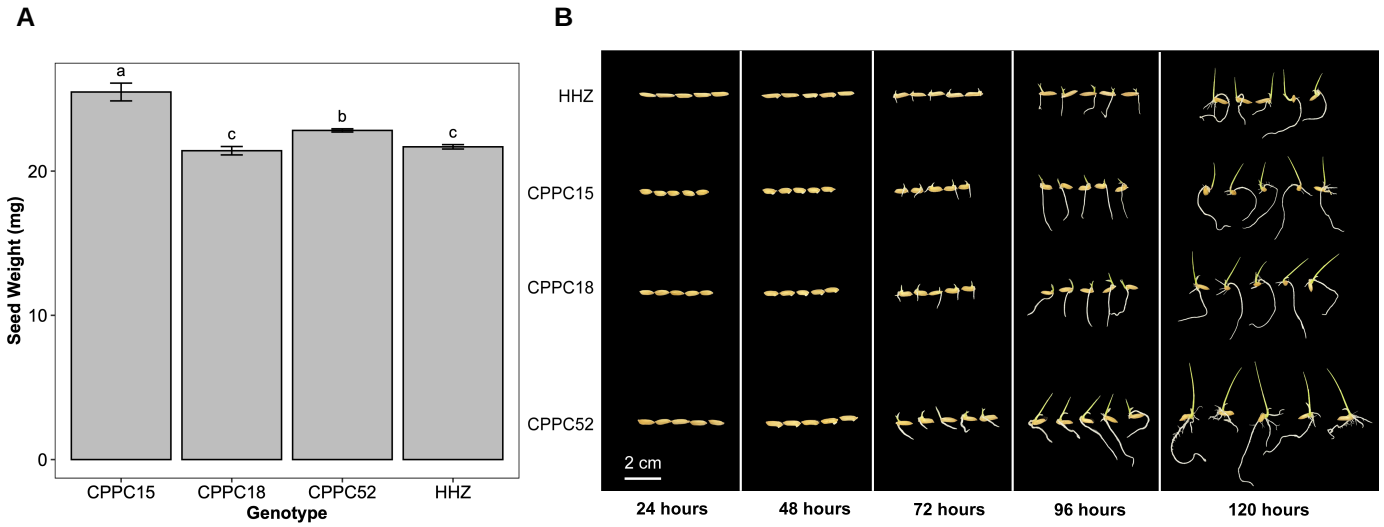

Fig. 1. Seed weight and seedling development. Seed weight (A) and seedling development during the first 5 d after sowing (B) of each genotype. For photographing seedling development, disinfected seeds of four varieties were placed in 15 cm diameter glass Petri dishes lined with two layers of filter paper and moistened with 25 ml of distilled water. The assay was conducted in a growth chamber at 28 °C under a 16 h light/8 h dark photoperiod. Different letters in (A) indicate statistically significant differences among genotypes (Tukey's HSD, $P<0.05$).

Where α is leaf absorbance, and β is the partitioning of absorbed quanta between PSII and PSI. Based on our previous studies (Xiong *et al.*, 2015a, 2017), a value of 0.425 was used for αβ.

The 'variable *J*' method was employed to calculate the CO_2 concentration inside chloroplasts (C_c) and mesophyll conductance (g_m):

$$C_c = \frac{\Gamma^* \times (\mathrm{ETR} + 8 \times (A + R_d))}{\mathrm{ETR} - 4 \times (A + R_d)}$$

$$g_m = \frac{A}{C_i - C_c}$$

where A and C_i are the steady-state photosynthetic rate and intercellular CO_2 concentration, respectively, directly taken from the gas exchange measurement. $\Gamma^\star$ is the CO_2 compensation point in the absence of respiration, and the typical value for rice, 40 μmol mol^{-1}, was used (Xiong *et al.*, 2015a, 2017). R_d is the daytime respiration rate, adapted from the light response curves. For each g_m calculation, we checked whether it met the reliability criterion ($10<dC_c/dA<50$).

Nitrogen content

After the gas exchange measurements, leaves were sampled to investigate LMA and nitrogen content. Leaf samples with known areas were dried at 80 °C to a constant weight, and LMA was calculated by dividing the leaf dry mass by the leaf area. The dry samples were then digested using the micro-Kjeldahl method (Xiong and Flexas, 2021), and the nitrogen concentrations were measured with a discrete wet chemistry analyzer (SmartChem 200, AMS-Westco, Rome, Italy).

Data analysis

In the current study, both the AGR and the RGR of biomass accumulation were estimated using two methods. First, the AGR was calculated based on biomass accumulation over two sampling periods. The average AGR between two sampling times was determined as $(M_2-M_1)/(t_2-t_1)$, and the average RGR between two sampling times was calculated as average $[\ln(M_2)-\ln(M_1)]/(t_2-t_1)$. Here, M_1 and M_2 represent the total biomass at times t_1 and t_2 (where $t_2>t_1$), respectively.

Second, the real-time AGR and RGR were estimated by fitting the biomass growth curve using the power model (Paine *et al.*, 2012):

$$M = [M_0^{1-\beta} + rt(1-\beta)]^{\frac{1}{1-\beta}}$$

where M represents the biomass at time t, M_0 represents the initial biomass, r is the intrinsic growth rate, which is crucial in determining the overall speed of the growth process, and β is a parameter that determines the shape of the growth curve (Supplementary Fig. S1). For different values of β, the curve can take various forms: if β is close to 1, the model behaves similarly to exponential growth; if $1>\beta>0$, the growth rate decreases as biomass increases, indicating a decelerating growth curve, and for the values of $\beta>1$, the growth rate increases as biomass increases. Based on the power model, the AGR dynamic with time is given by:

$$AGR = r[M_0^{1-\beta} + rt(1-\beta)]^{\frac{1}{1-\beta}}$$

The RGR dynamic with time is given by:

$$RGR = \frac{r}{M_0^{1-\beta} + rt(1-\beta)}$$

Similarly, RGR dynamic with mass (RGR_s) is given by:

$$RGR_s = rM^{\beta-1}$$

The net assimilation rate (NAR) of the plants was estimated using the formulation proposed by Hunt (1982), expressed as: RGR=LAR×NAR. Since leaf mass and leaf area dynamics were not modeled over time, NAR was calculated directly from paired harvests. Specifically, RGR was determined from the logarithmic increase in total biomass between two successive sampling dates, while the leaf area ratio (LAR) was obtained as the average of the ratios of leaf area to total biomass at those

two dates. The ratio of RGR to mean LAR was then used to estimate NAR for each growth interval.

In the current study, all the analyses were conducted, and results were visualized using R version 4.4.1 (R Core Team, 2024). The R package 'nlme' was used to fit the power growth model and simulate both real-time AGR and RGR. One-way ANOVA was employed to assess the differences in measured traits between genotypes, with Tukey's test used for pairwise comparisons at the 0.05 significance level, utilizing the 'multcomp' package. The standardized major axis (SMA) analysis was conducted to examine the correlations between traits using the 'smatr' package. The 'tidyverse', a collection of open-source packages, along with 'dplyr', 'cowplot', and 'readxl' packages, were used for data analysis and visualization.

Results

Early growth

Plant growth was monitored under both pot and field conditions. The pot experiment allowed frequent destructive sampling and detailed physiological measurements, whereas the field experiment was conducted to verify whether the observed growth patterns were consistent under agronomic conditions. Therefore, Fig. 2 presents data from the pot experiment, while the corresponding field results are shown in Supplementary Fig. S3. Both experiments consistently showed that the newly developed lines accumulated biomass more rapidly than HHZ during the early growth stage. The three newly developed rice lines exhibited faster biomass accumulation (shoot and root) than the common commercial variety, HHZ, under both conditions. The differences in biomass among the three newly developed rice lines were not significant for most sampling days under pot conditions, although CPPC52 showed slightly higher biomass accumulation under field conditions. These newly developed lines also showed greater plant height during the early growth stage in both pot and field conditions.

Leaf area per plant was also significantly higher in the newly developed lines than in HHZ during the early growth stage (Fig. 2; Supplementary Fig. S3). Under pot conditions, the CPPC lines maintained a larger leaf area than HHZ over the first 36 d after sowing, although these differences diminished by 43 d as canopy closure was approaching. Under field conditions, leaf area differences among genotypes were smaller, but CPPC52 still exhibited a significantly larger leaf area than the other genotypes (Supplementary Fig. S4). In addition to greater biomass and leaf area, the newly developed lines showed increased plant height during early growth under both pot and field conditions (Fig. 2; Supplementary Fig. S4). In contrast, tiller numbers showed no clear pattern, although HHZ had the highest tiller number under field conditions. To compare the relative importance of different growth traits, plant height, tiller number, biomass, and leaf area were normalized for each genotype (Supplementary Fig. S4). This analysis showed that variation in biomass and leaf area contributed far more strongly to early growth differences than variation in plant height or tiller number.

Growth rate over the early growth period

As expected, the average AGR for all genotypes under both pot and field conditions increased significantly with the days after sowing; however, the average RGR values, which were estimated based on the assumption that biomass accumulation is exponential with respect to days after sowing, fluctuated between the sampled periods and showed no clear pattern among genotypes (Supplementary Figs S5–S7). Consistent with the estimations of the average RGR values, the relationship between natural logarithm-transformed biomass and days after sowing (Fig. 3) was clearly non-linear for all genotypes. Therefore, we investigated the temporal dynamics of AGR and RGR by fitting a growth model. The power model provided an excellent fit to the biomass accumulation data for all genotypes, as indicated by high R^2 values and favorable AIC (Akaike information criterion) and BIC (Bayesian information criterion) statistics (Table 1; Supplementary Figs S7, S8). Surprisingly, the exponent parameter, β, for HHZ was close to 1, while the fitted β values for our newly developed lines ranged from 0.760 to 0.875. The intrinsic growth rate (r), which is crucial in determining the overall speed of the growth process, is larger for newly developed lines than for HHZ.

Using the fitted parameters for each genotype, we simulated the temporal dynamics of AGR and RGR over the early growth stage (Fig. 4). The newly developed rice lines showed higher AGR and RGR over the first 40 d. Consistent with the average growth rates described above, AGR increased as the days after sowing increased, with each genotype showing similar trends but different absolute values. RGR decreased over time for all genotypes, and the differences in initial RGR and the rate of decline highlight the specific growth characteristics of each genotype. CPPC15 and CPPC18 started with higher RGRs but declined rapidly, while CPPC52 and HHZ started with lower RGRs but declined more slowly. Indeed, HHZ maintained the lowest RGR throughout the period, suggesting it has a more consistent, albeit slower, growth pattern.

Testing the associations of relative growth rate with plant biomass allocations

Given the significant differences in RGR observed among genotypes within 30 d after sowing, we first investigated the factors underlying these differences from the perspective of carbon allocation. As shown in Fig. 5A, the biomass distribution between roots and shoots varied significantly across genotypes. During the early stage of growth, HHZ allocated almost half of its biomass to the root system, whereas the newly developed lines allocated much less biomass to their root systems. We further analyzed the allometric relationships between shoot and root biomass using standardized major axis regression (Fig. 5B). In all genotypes, shoot biomass increased more rapidly than root biomass, indicating a general tendency for greater

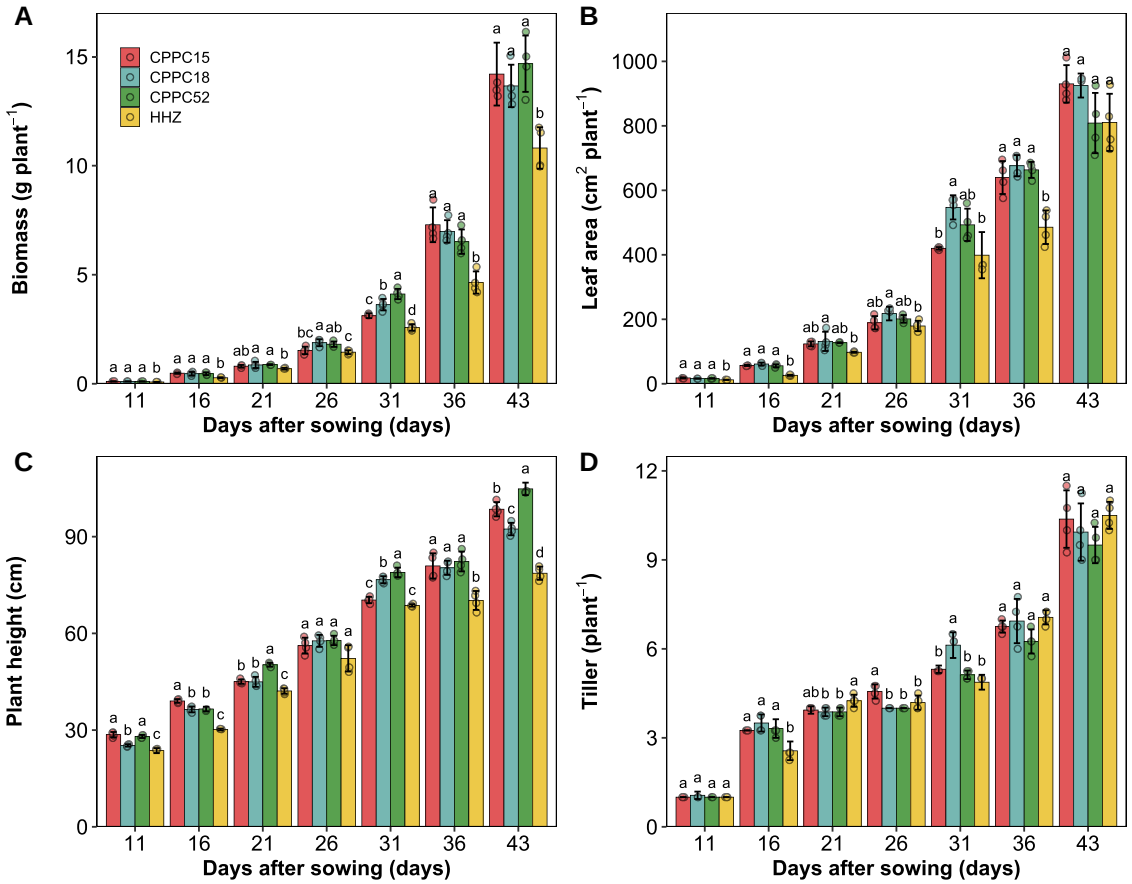

Fig. 2. Rice plant growth performance in pot conditions. The bars represent mean values (±SE, $n = 4$), while the open points indicate pooled data for each genotype. The letters near the bars denote significant differences between genotypes ($P<0.05$; Tukey's HSD after ANOVA).

allocation to above-ground tissues during early development. However, both the slopes and elevations of the allometric relationships differed significantly between HHZ and the newly developed lines. The high leaf biomass of these lines was closely related to their larger leaf area (Fig. 2), which was mainly due to the increased width of the leaves rather than their length (Fig. 6). The correspondence between biomass allocation patterns and growth dynamics was particularly clear when comparing RGR with leaf biomass and leaf area. Genotypes that allocated a larger fraction of biomass to leaves exhibited higher RGR during early development, whereas greater allocation to roots was associated with lower RGR.

Testing the associations of relative growth rate with photosynthetic traits

To investigate whether the leaf assimilation rate contributes to the high RGR of newly developed lines, we estimated both light response curves and CO_2 response curves in pot conditions between 16 d and 20 d after sowing. As shown in Fig. 7A, the light response curves of the four genotypes are very similar, although the net photosynthetic rate (P_n) of HHZ at high light intensities was slightly higher than that of the newly developed lines. The parameters derived from the light response curves (Table 2), including the light-saturated photosynthetic rate (A_{sat}), quantum yield (Φ), light compensation point (LCP), and light intensity at 75% saturation of photosynthesis, showed no significant differences between HHZ and the newly developed lines, except for the A_{sat} of CPPC18 and the LCP of CPPC15.

The steady-state gas exchange at ambient conditions, with a CO_2 concentration of 400 ppm and a light intensity of 1500 μmol m^{-2} s^{-1}, showed that the steady-state photosynthetic rate (A) was higher in HHZ than in the newly developed lines (Table 2). Regarding other photosynthetic traits, the mesophyll conductance (g_m) of HHZ was significantly higher than that of the newly developed lines, and its stomatal conductance (g_s), CO_2 concentration inside chloroplasts (C_c), and electron transport rate (ETR) were higher than those of CPPC15 but not of the other lines. Interestingly, the CO_2 response curve of HHZ differed distinctly from that of the newly developed lines (Fig. 7B; Supplementary Fig. S9). HHZ exhibited the highest photosynthetic rates across almost all CO_2 concentrations, reaching a plateau faster and at a higher rate

compared with the newly developed lines. As a result, the fitted maximum carboxylation rate (V_{cmax}) and maximum electron transport rate (J_{max}) were significantly higher in HHZ than in other genotypes. The high V_{cmax} and J_{max} of HHZ are likely to be due to the high leaf nitrogen content (Table 2). Consistently, leaf nitrogen content expressed on an area basis was significantly higher in HHZ (1.11 g m^{-2}) than in the CPPC lines (0.81–0.84 g m^{-2}). LMA also differed among genotypes, with CPPC18 and HHZ showing a higher LMA than CPPC15 and CPPC52. In the current study, we also estimated the net assimilation rate (Fig. 7C), and in agreement with the leaf-level CO_2 assimilation patterns, the net assimilation rate in HHZ was higher than that of the CPPC lines during the same growth period that gas exchange was estimated; however, these genotypic differences diminished progressively with increasing days after sowing. By contrast, the leaf mass fraction was greater in the CPPC lines than in HHZ at the initial stages, yet this disparity disappeared by 21 d after sowing (Fig. 5).

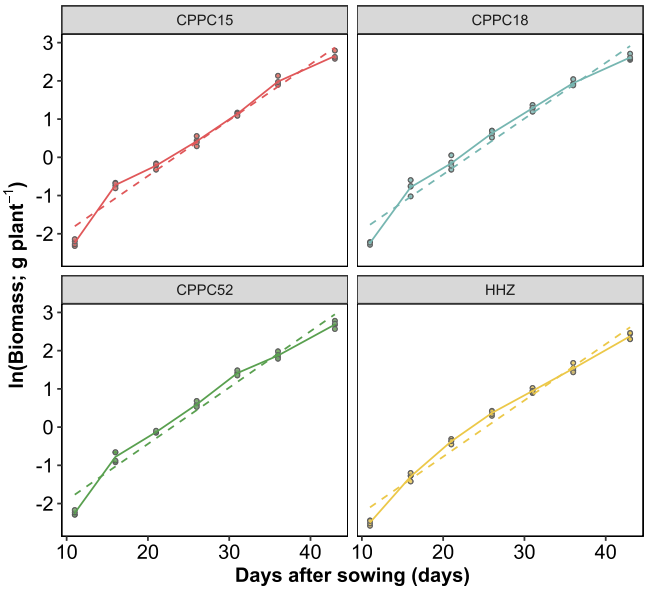

Fig. 3. Natural logarithm-transformed biomass plotted against days after sowing. In the context of an exponential growth model, the slopes of the line segments on semi-logarithmic plots represent the relative growth rate (RGR). The solid line segments show the inferred slopes if the plants grow exponentially throughout each census period. The dashed lines represent the constant RGR derived from fitting an exponential growth model to the entire dataset. Biomass measurements were collected from pot-grown plants as shown in Fig. 2A.

Discussion

Relative growth rate is not constant during the early growth stage

Growth analysis is a commonly used approach for quantifying plant growth. While it is well established that the RGR of plants typically changes over their ontogeny, calculations of RGR for comparative purposes, especially over shorter intervals typical of early growth studies, have often relied on methods assuming or simplifying to an average rate, sometimes based on an underlying exponential growth model (Evans, 1972; Hunt, 1982; Fletcher *et al.*, 2022). In practice, many studies estimate RGR by harvesting plants at only two harvest points and calculating it using the difference in natural logarithms of biomass measurements divided by the time interval between harvests (Osone *et al.*, 2008; Rebolledo *et al.*, 2012; Fletcher *et al.*, 2022). When more than two measurements are available, RGR is sometimes estimated as the slope of a linear regression of natural logarithms of biomass measurements against time (Paine *et al.*, 2012; Pommerening and Muszta, 2016; Lamont *et al.*, 2023).

The exponential growth model implicitly assumes a proportional increase in carbon acquisition capacity with biomass accumulation. In higher plants, however, this assumption is rarely met because newly accumulated dry matter is increasingly allocated to non-photosynthetic tissues, while leaf self-shading (Poorter *et al.*, 2012; Hilty *et al.*, 2021) and structural heterogeneity reduce the efficiency of carbon gain (Xiong *et al.*, 2015a, b). Consequently, respiration costs increase with the total biomass of the plant, while carbon acquisition scales only with photosynthetic biomass. As a result, the biomass accumulation rate, relative to total biomass, decreases as plants grow. In this study, we harvested plants seven times over the initial 43 d to dissect the nuanced differences in early vigor. We showed that average RGR values calculated between different harvest intervals fluctuated and did not provide a clear, consistent distinction between genotypes across all periods. In addition to differences in RGR, the CPPC lines also showed higher AGRs during the early establishment phase once canopy leaf

Table 1. Power model parameter estimates and statistical metrics for biomass (M) by genotype

Genotype	M_0	R	β	AIC	BIC	R^2
CPPC15	(1.33±3.98)×10^{-13}	0.184±0.034	0.763±0.096	60.9	66.2	0.983
CPPC18	(5.93±7.70)×10^{-5}	0.172±0.020	0.760±0.062	35.3	40.6	0.993
CPPC52	(1.88±3.19)×10^{-2}	0.147±0.022	0.875±0.077	49.4	54.7	0.989
HHZ	(3.16±3.38)×10^{-2}	0.132±0.017	0.944±0.078	30.9	36.2	0.989

The power model is expressed as $M(t) = [M_0^{1-\beta} + rt(1-\beta)]^{1/(1-\beta)}$. For each genotype, three parameters, M_0, r, and β, were estimated, along with the AIC, BIC, and the coefficient of determination (R^2). The parameter are expressed as means ±SEs.

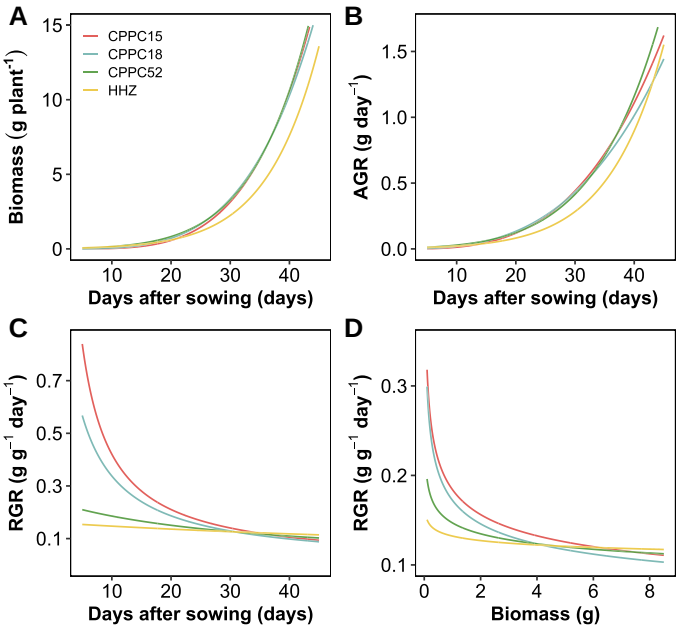

Fig. 4. Fitted values from the power model. Fitted values from the power model for (A) biomass, (B) absolute growth rate (AGR), (C) relative growth rate (RGR) on a time basis, and (D) RGR on a biomass basis (RGR_s) for four estimated genotypes. The parameters used for fitting each genotype are provided in Table 1.

area expanded, indicating that their advantage was not limited to size-normalized growth efficiency but also translated into greater absolute biomass accumulation. The non-linearity between natural logarithm-transformed biomass and time (Fig. 3) underscores that a single average RGR, while providing a mean value, cannot fully capture the dynamic nature of growth crucial for early establishment and competition. Dynamics can differentiate genotypes in ways an overall average might obscure.

Growth models are categorized into two main types: those that assume an asymptotic final size and those that do not (Paine *et al.*, 2012). The concept of an asymptotic final size is well established in population growth but is more complex for individual plants. Plant growth may reach an asymptote due to limited resources or ontogenetic changes, such as flowering (Hilty *et al.*, 2021). The choice between asymptotic and non-asymptotic models depends on the response variable and study time frame. Asymptotic models are suitable for studies covering the entire life span, whereas non-asymptotic models, which assume indefinite growth, are useful for early growth stages, such as seedlings. Indeed, the early biomass growth of rice fits very well with a power model, a non-asymptotic model, as indicated by BIC, AIC, and R^2 values (Fig. 4; Table 1). Based on the fitted parameters, it is evident that all fitted exponents, β, are <1, indicating that the early growth of rice is not exponential. Moreover, the β values for all newly developed lines were smaller than for HHZ, indicating a faster RGR reduction with growth. Calculations using the power model further demonstrated that the RGR of rice seedlings is highly dynamic and far from constant. Interestingly, the fitted parameter, *r*, which represents an intrinsic growth rate, is likely to be used as an index of RGR, and clearly more investigations are required. Moreover, the empirically derived *r* and β parameters from the growth model, along with the observed biomass allocation pattern, offer additional inputs for the development of more sophisticated integrative analyses. This indicates that crop growth models may need to account for genotype-specific allocation and canopy development strategies rather than assuming a uniform relationship between leaf area and photosynthetic capacity. These parameters can facilitate advanced modeling approaches, such as three-dimensional architectural frameworks or resource allocation models (e.g. Chang *et al.*, 2019), aimed at elucidating the roles of canopy development and resource utilization in promoting early vigor across varying environmental conditions. It should also be noted that fluctuations in weather, from short-term dynamics to seasonal variation, probably contributed to growth variation, yet their specific effects could not be disentangled in the present study.

New lines with rapid early growth allocate more biomass to leaves than roots

As shown in Fig. 5, the newly developed lines allocated a greater proportion of biomass to leaves and a smaller proportion to roots than HHZ during the early sampling stages. This contrast was most pronounced at the onset of growth and gradually diminished as plants developed. The temporal pattern of biomass partitioning closely tracked changes in RGR, indicating that early growth is strongly associated with how carbon is distributed among plant organs (Poorter *et al.*, 2012; Monson *et al.*, 2022). This allocation pattern reflects a fundamental trade-off between investment in canopy development and investment in below-ground resource acquisition. In the newly developed lines, preferential allocation of carbon to leaves promotes rapid canopy expansion and early light interception, thereby increasing whole-plant carbon gain. At the same time, reduced allocation to roots implies lower investment in nutrient and water uptake capacity. In this context, strategic allocation refers to consistent, genotype-dependent patterns of carbon partitioning that balance rapid canopy development against resource acquisition.

Although grain yield was not directly measured, early biomass accumulation strongly influences canopy closure, weed suppression, and radiation interception, all of which are closely linked to yield formation in direct seeded and short-season rice systems (Pan *et al.*, 2023; Yang *et al.*, 2024). The canopy expansion strategy observed in the new lines is therefore expected to confer agronomic advantages by enhancing early season productivity. This strategy, however, is associated with clear costs. Reduced investment in root systems may constrain nitrogen

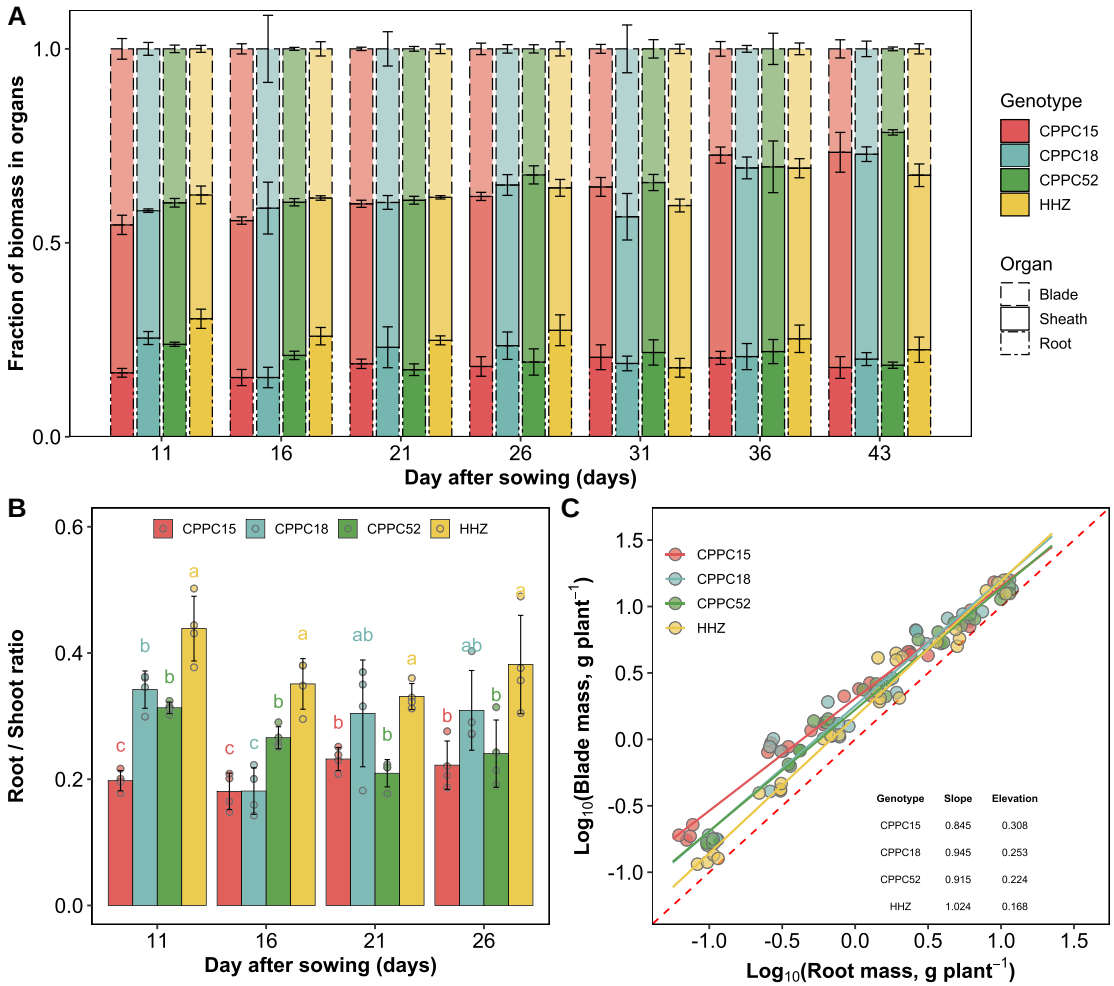

Fig. 5. Biomass allocation between organs. (A) The fraction of biomass allocation in different organs, (B) root to shoot ratio, and (C) biomass allometric relationships between leaf and root mass for four genotypes. The bars in (A) and (B) represent mean values (±SE, $n = 4$), and the open points in (C) indicate data points for each genotype. The letters near the bars denote significant differences between genotypes ($P<0.05$; Tukey's HSD after ANOVA). The solid lines in (C) represent the standard major axis (SMA) regression fit for each genotype, and the red dashed line represents the 1:1 line. The SMA slope describes the scaling between root and leaf mass, while the elevation corresponds to the intercept of the regression. Different letters indicate significant differences between genotypes in slope or elevation.

uptake capacity and probably contributes to the lower leaf nitrogen content observed in the newly developed lines. The increased allocation to roots at later stages may therefore represent a functional adjustment to intensifying competition for water and nitrogen as plant size and canopy density increase. Clearly, future studies are required to investigate the impacts of the biomass allocation strategies on RGR under multiple environmental conditions.

Rapid early growth reflects a trade-off between canopy expansion and leaf-level photosynthetic efficiency

The newly developed lines achieved higher early RGRs not by enhancing photosynthetic capacity per unit leaf area, but by prioritizing rapid canopy expansion through increased biomass allocation to leaves and morphological enlargement of leaf blades. This trade-off maximizes whole-plant carbon gain via enhanced light interception, even though photosynthetic efficiency per unit area is reduced (Xiong, 2024). Greater plant height, together with larger leaf area, further contributes to faster canopy closure and improved light interception. However, stem investment primarily supports leaf display rather than directly contributing to carbon assimilation, representing an additional structural cost of rapid canopy development (Chang *et al.*, 2019). Early vigor therefore reflects a coordinated investment in leaf area, stem support, and reduced below-ground allocation.

The high canopy leaf area in the new developed lines is due to the large leaf area rather than the number of leaves per tiller. Our results show that the large leaves in the newly developed

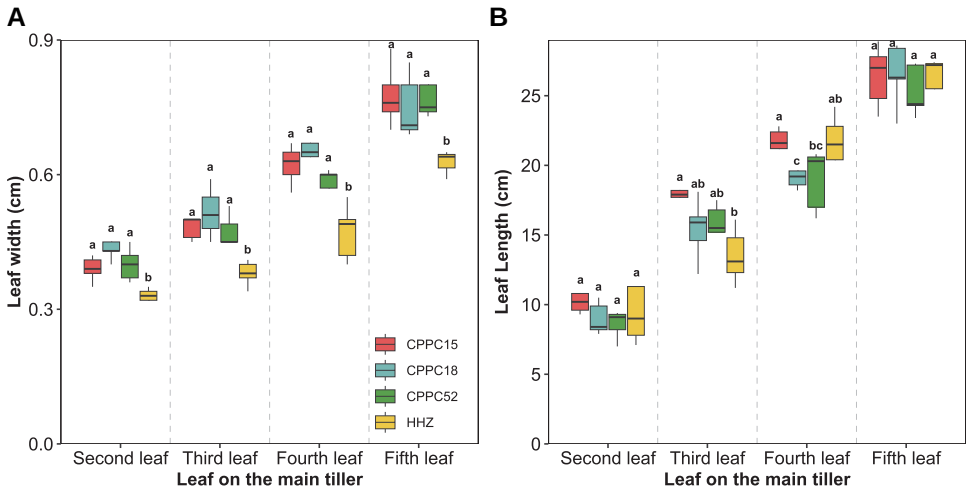

Fig. 6. Leaf blade width and length. The blade width (A) and length (B) of the first four complete leaves for each genotype. Leaf widths were measured at the middle of the leaf. Note: the first leaf has only a sheath and is considered an incomplete leaf. Different letters indicate statistically significant differences (P<0.05; Tukey's HSD after ANOVA) between genotypes.

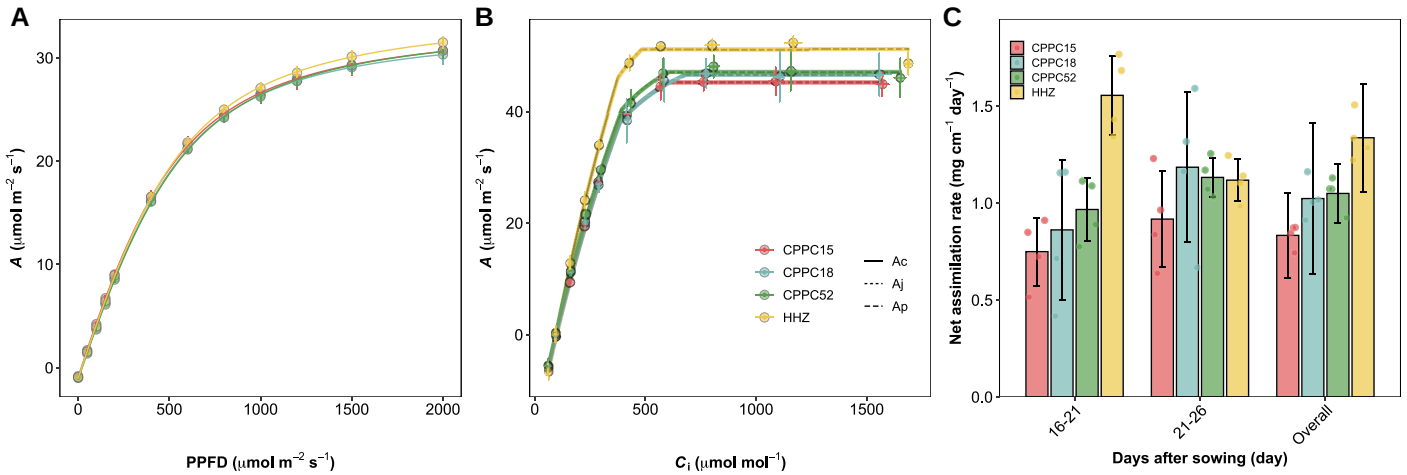

Fig. 7. Response curves of the CO_2 assimilation rate and growth rate components in four rice genotypes. (A) Response of A to photosynthetic photon flux density (PPFD) and (B) to intercellular CO_2 concentration (C_i) for each genotype. A_c, A_j, and A_p indicate the limitations on A due to ribulose bisphosphate (RuBP) carboxylation, RuBP regeneration, and the availability of inorganic phosphate, respectively. The open points in (A) and (B) represent mean values (±SE, n = 6). Details about the fitted parameters for CO_2 assimilation curves are shown in Table 2. Asterisks indicate significant differences in photosynthetic rates between genotypes at a specific PPFD or ambient CO_2 concentrations based on ANOVA. *P<0.05; **P<0.005; ***P<0.001. (C) The average net assimilation rate from 16 to 21 d after sowing, from 21 to 26 d after sowing, and the overall period. Bars in (C) represent mean values (±SE, n=4) and points near the bar represent the individual measurements. Different letters above the bars indicate significant differences among genotypes (P<0.05).

lines are mainly due to increased leaf width rather than length. The finding is consistent with the observations in wheat (Zhang *et al.*, 2015). While we identified increased leaf width as a key morphological determinant of larger leaf area in the rapidly growing lines, the cellular and physiological mechanisms driving this enhanced lateral growth remain to be elucidated. Future research could profitably explore aspects such as cell division and expansion rates within the leaf blade, the role of plant hormones known to influence leaf morphology (Jathar *et al.*, 2022; Huang *et al.*, 2023), or differences in turgor pressure and cell wall properties that might facilitate preferential widening over elongation (Coussement *et al.*, 2021; Ali *et al.*, 2023).

Selecting wider leaves as a rapid growth trait in rice may offer specific advantages, although it also requires additional vascular and structural investment. Compared with leaf elongation, which demands sustained longitudinal vascular development, mechanical support, and strong hormonal control, lateral

Table 2. Leaf morphological, biochemical, and photosynthetic traits of newly developed leaves measured 16–20 d after sowing

Genotype	CPPC15	CPPC18	CPPC52	HHZ
A_{sat} (μmol m^{-2} s^{-1})	35.0±1.3 ab	34.5±1.3 b	35.2±1.1 ab	36.1±0.8 a
Φ (μmol mol^{-1})	0.055±0.002 a	0.053±0.002 a	0.053±0.002 a	0.054±0.001 a
θ (unitless)	0.73±0.03 a	0.76±0.03 a	0.75±0.01 a	0.74±0.02 a
LCP (μmol m^{-2} s^{-1})	17.3±0.8 b	20.3±1.3 a	22.3±1.2 a	19.5±1.8 ab
Q_{sat_75} (μmol m^{-2} s^{-1})	955±63 a	941±56 a	999±27 a	988±58 a
R_d (μmol m^{-2} s^{-1})	0.94±0.05 b	1.06±0.08 a	1.17±0.07 a	0.96±0.11ab
A (μmol m^{-2} s^{-1})	29.2±0.9 b	29.1±1.9 b	30.6±1.2 b	34.6±1.6 a
g_s (mol m^{-2} s^{-1})	0.36±0.01b	0.44±0.03 a	0.45±0.02 a	0.44±0.04 a
C_i (μmol mol^{-1})	288±4 b	295±7 ab	302±3 a	289±3 ab
g_m (mol m^{-2} s^{-1})	0.33±0.05 b	0.35±0.05 b	0.32±0.03 b	0.45±0.05 a
C_c (μmol mol^{-1})	193±12 b	208±9 a	204±4 ab	210±6 a
ETR (μmol m^{-2} s^{-1})	211±4 b	219±9 ab	223±9 a	230±6 a
V_{cmax} (μmol m^{-2} s^{-1})	118±13 b	119±6 b	122±9 b	145±12 a
J_{max} (μmol m^{-2} s^{-1})	338±14 c	337±9 c	360±10 b	393±27 a
Leaf N (g m^{-2})	0.84±0.16 b	0.84±0.06 b	0.81±0.14 b	1.11±0.02 a
LMA (g m^{-2})	22.9±0.5 b	25.2±0.4 a	23.5±0.1 b	25.1±0.3 a

A_{sat}, light-saturated photosynthetic rate fitted from light response curves; Φ, quantum yield; θ, *a* unitless parameter that affects the shape of the light response curve; LCP, light compensation point; Q_{sat_75}, light intensity at 75% saturation of photosynthesis; R_d, daytime respiration rate; A, steady-state photosynthetic rate at ambient CO_2 concentration; g_s, stomatal conductance to CO_2; C_i, intercellular CO_2 concentration; g_m, mesophyll conductance to CO_2; C_c, CO_2 concentration inside chloroplasts; ETR, electron transport rate; V_{cmax}, maximum carboxylation rate; J_{max}, maximum electron transport rate; LMA, leaf mass per area. Data are shown as means ±SE (n=4–6). Different letters indicate statistically significant differences (P<0.05; Tukey's HSD after ANOVA) between genotypes.

expansion may involve a different balance of structural and biochemical costs (Skinner and Nelson, 1995; Baird *et al.*, 2021). Leaf widening can occur simultaneously along the entire blade (Durand, 1999; Baird *et al.*, 2021), whereas elongation depends on progressive growth from the base and faces stronger developmental and transport constraints (Nelson and Dengler, 1997; Ocheltree and Gleason, 2024). Moreover, leaf width appears to have greater genetic plasticity than leaf length, which is more tightly constrained by overall plant architecture (Zhang *et al.*, 2015).

Although the leaf photosynthetic rate cannot directly translate into whole-plant carbon gain, many canopy characteristics (e.g. leaf angle and leaf area distribution), which were not estimated in the present study, can influence the canopy photosynthetic rate (Chang *et al.*, 2019). We found that the leaf photosynthetic rates of the newly developed lines were lower than those of HHZ. Consistently, both the light response curve and CO_2 response curve of HHZ were higher than those of the newly developed lines (Fig. 7). Photosynthesis in C_3 plants is limited by photosynthetic biochemical processes and photosynthetic CO_2 diffusion, including stomatal (g_s) and mesophyll (g_m) conductance (Xiong, 2023). In the newly developed lines, the biochemical capacity for photosynthesis, represented by V_{cmax} and J_{max}, was significantly lower than in HHZ. Leaf nitrogen content largely determines the potential for both parameters because nitrogen is a major component of photosynthetic proteins (Walker *et al.*, 2014; Xiong and Flexas, 2018). Consistently, the leaf nitrogen contents were much lower in the newly developed lines than in HHZ. The lower leaf nitrogen content may be caused by the diluting effect of the larger leaves of the newly developed lines and/or the lower nitrogen uptake capacity due to their smaller root systems (Shi *et al.*, 2020).

In addition, g_m was consistently lower in the newly developed lines, representing an additional limitation to CO_2 diffusion. Previous studies have shown that g_m is closely linked to leaf nitrogen content and its distribution among leaf tissues and cellular components (Xiong *et al.*, 2015a; Xiong and Flexas, 2018; Xiong, 2023). Together, the lower leaf nitrogen concentration and altered LMA of the newly developed lines indicate a clear physiological cost of rapid leaf area expansion. Rapid morphological growth dilutes nitrogen investment per unit leaf area and limits allocation to photosynthetic proteins, resulting in reduced V_{cmax} and J_{max}. Lower nitrogen availability within the mesophyll is also likely to contribute to the reduced g_m. By comparison, the higher leaf nitrogen content and LMA of HHZ indicate a strategy of investing assimilated carbon into thicker, more photosynthetically efficient leaves rather than into rapid expansion of total leaf area (Table 2). Nitrogen economy therefore represents a central trade-off in early vigor; that is, accelerated canopy expansion is achieved at the expense of photosynthetic biochemical capacity and CO_2 diffusion efficiency.

Conclusions

Rapid early crop growth, commonly referred to as early seedling vigor, is critical for timely canopy establishment and

efficient resource capture. These processes enhance crop competitiveness against weeds and support productivity in cropping systems characterized by shortened growth periods. Although water use efficiency and nitrogen use efficiency were not directly quantified in this study, our results indicate that the canopy expansion strategy increases whole-plant carbon gain, while nitrogen dilution may constrain nitrogen use efficiency at the leaf level. This study demonstrates that rapid early growth in rice can be achieved not through increased photosynthetic capacity per unit leaf area, but through the prioritization of canopy expansion driven by leaf morphological development and biomass allocation. This strategy entails clear trade-offs, including reduced nitrogen investment per unit leaf area, lower photosynthetic biochemical capacity, and reduced mesophyll conductance. Despite these costs, it leads to higher whole-plant biomass productivity during early establishment.

Our findings challenge the prevailing assumption that rapid growth is inherently linked to elevated leaf-level photosynthesis. Instead, they identify canopy expansion as a dominant determinant of early vigor. More broadly, the results underscore the importance of dynamic growth trajectories, biomass allocation patterns, and leaf morphological traits in shaping early growth performance. Together, these insights provide a conceptual framework for rice improvement programs that aim to enhance early vigor by targeting traits related to canopy development rather than focusing exclusively on photosynthetic efficiency. Future studies that integrate physiological measurements with genetic, cellular, and modeling approaches will be essential for elucidating the mechanisms underlying these strategies and for evaluating their robustness across diverse environmental and management conditions.

Supplementary data

The following supplementary data are available at *JXB* online

Fig. S1. Conceptual illustration of the power-law growth model.
Fig. S2. Environmental conditions during the experiment.
Fig. S3. Rice plant growth performance under field conditions.
Fig. S4. Normalized plant growth after seed sowing.
Fig. S5. The absolute relative growth rate between sampling intervals.
Fig. S6. The average relative growth rate between sampling intervals.
Fig. S7. The average absolute and relative growth rate between sampling intervals.
Fig. S8. Plant growth curves fitted with a power growth function based on empirical biomass data over time.
Fig. S9. Response curves of the CO_2 assimilation rate to intercellular CO_2 concentration for each genotype.

Acknowledgements

We thank Miss Ningyu Liu and Dr Zhenmei Wang for their help in conducting experiments and correcting the manuscript.

Author contributions

YZ: carried out the research; YZ and DX: analyzed the data; DX: designed the research and wrote the manuscript; YZ, DX, XY, XL, KC, JH, and SP: revised the manuscript. All authors read and approved the final manuscript.

Conflict of interest

The authors have no conflicts to declare.

Funding

Research in our lab is supported by the Earmarked Fund for China Agriculture Research System (CARS-01), and Fundamental Research Funds for the Central Universities (2662025PY028, 2662024QH005, and 2662025YJ014).

Data availability

The primary data supporting this study were not made publicly available at the time of publication. Data will be made available upon request to the corresponding author.

References

Aharon S, Fadida-Myers A, Nashef K, Ben-David R, Lati RN, Peleg Z. 2021. Genetic improvement of wheat early vigor promote weed-competitiveness under Mediterranean climate. Plant Science **303**, 110785.

Ali O, Cheddadi I, Landrein B, Long Y. 2023. Revisiting the relationship between turgor pressure and plant cell growth. New Phytologist **238**, 62–69.

Baird AS, Taylor SH, Pasquet-Kok J, *et al.* 2021. Developmental and biophysical determinants of grass leaf size worldwide. Nature **592**, 242–247.

Blackman VH. 1919. The compound interest law and plant growth. Annals of Botany **33**, 353–360.

Cairns JE, Namuco OS, Torres R, Simborio FA, Courtois B, Aquino GA, Johnson DE. 2009. Investigating early vigour in upland rice (*Oryza sativa* L.): part II. Identification of QTLs controlling early vigour under greenhouse and field conditions. Field Crops Research **113**, 207–217.

Chang T-G, Zhao H, Wang N, Song Q-F, Xiao Y, Qu M, Zhu X-G. 2019. A three-dimensional canopy photosynthesis model in rice with a complete description of the canopy architecture, leaf physiology, and mechanical properties. Journal of Experimental Botany **70**, 2479–2490.

Coussement JR, Villers SLY, Nelissen H, Inzé D, Steppe K. 2021. Turgor-time controls grass leaf elongation rate and duration under drought stress. Plant, Cell & Environment **44**, 1361–1378.

Duan T, Chapman SC, Holland E, Rebetzke GJ, Guo Y, Zheng B. 2016. Dynamic quantification of canopy structure to characterize early plant vigour in wheat genotypes. Journal of Experimental Botany **67**, 4523–4534.

Durand J. 1999. Grass leaf elongation rate as a function of developmental stage and temperature: morphological analysis and modelling. Annals of Botany **83**, 577–588.

Evans GC. 1972. The quantitative analysis of plant growth. Oxford: Blackwell Scientific Publications.

Fletcher LR, Scoffoni C, Farrell C, Buckley TN, Pellegrini M, Sack L. 2022. Testing the association of relative growth rate and adaptation to climate across natural ecotypes of *Arabidopsis*. New Phytologist **236**, 413–432.

Gu J, Yang J. 2022. Nitrogen (N) transformation in paddy rice field: its effect on N uptake and relation to improved N management. Crop and Environment **1**, 7–14.

He J, Ma J, Cao Q, Wang X, Yao X, Cheng T, Zhu Y, Cao W, Tian Y. 2022. Development of critical nitrogen dilution curves for different leaf layers within the rice canopy. European Journal of Agronomy **132**, 126414.

Hilty J, Muller B, Pantin F, Leuzinger S. 2021. Plant growth: the what, the how, and the why. New Phytologist **232**, 25–41.

Huang P, Zhao J, Hong J, Zhu B, Xia S, Zhu E, Han P, Zhang K. 2023. Cytokinins regulate rice lamina joint development and leaf angle. Plant Physiology **191**, 56–69.

Hunt R. 1982. Plant growth curves: the functional approach to plant growth analysis. London: Edward Arnold.

Jathar V, Saini K, Chauhan A, Rani R, Ichihashi Y, Ranjan A. 2022. Spatial control of cell division by GA–OsGRF7/8 module in a leaf explaining the leaf length variation between cultivated and wild rice. New Phytologist **234**, 867–883.

Lamont BB, Williams MR, He T. 2023. Relative growth rate (RGR) and other confounded variables: mathematical problems and biological solutions. Annals of Botany **131**, 555–568.

Liao M, Fillery IRP, Palta JA. 2004. Early vigorous growth is a major factor influencing nitrogen uptake in wheat. Functional Plant Biology **31**, 121–129.

Monson RK, Trowbridge AM, Lindroth RL, Lerdau MT. 2022. Coordinated resource allocation to plant growth–defense tradeoffs. New Phytologist **233**, 1051–1066.

Nelson T, Dengler N. 1997. Leaf vascular pattern formation. The Plant Cell **9**, 1121–1135.

Ocheltree TW, Gleason SM. 2024. Grass veins are leaky pipes: vessel widening in grass leaves explain variation in stomatal conductance and vessel diameter among species. New Phytologist **241**, 243–252.

Osone Y, Ishida A, Tateno M. 2008. Correlation between relative growth rate and specific leaf area requires associations of specific leaf area with nitrogen absorption rate of roots. New Phytologist **179**, 417–427.

Paine CET, Marthews TR, Vogt DR, Purves D, Rees M, Hector A, Turnbull LA. 2012. How to fit nonlinear plant growth models and calculate growth rates: an update for ecologists. Methods in Ecology and Evolution **3**, 245–256.

Pan X-C, Yang G-D, Fu Y-Y, Wang X-Y, Xiong Q, Xu L, Peng S-B. 2023. Yield performance and agronomic characteristics of a newly developed ultrashort-duration line in direct-seeded double-season rice system. Acta Agronomica Sinica **49**, 2738–2752.

Pommerening A, Muszta A. 2016. Relative plant growth revisited: towards a mathematical standardisation of separate approaches. Ecological Modelling **320**, 383–392.

Poorter H, Niklas KJ, Reich PB, Oleksyn J, Poot P, Mommer L. 2012. Biomass allocation to leaves, stems and roots: meta-analyses of interspecific variation and environmental control. New Phytologist **193**, 30–50.

R Core Team. 2024. R: a language and environment for statistical computing. Vienna, Austria: R Foundation for Statistical Computing. https://www.R-project.org/.

Rebetzke GJ, Richards RA, Fettell NA, Long M, Condon AG, Forrester RI, Botwright TL. 2007. Genotypic increases in coleoptile length improves stand establishment, vigour and grain yield of deep-sown wheat. Field Crops Research **100**, 10–23.

Rebolledo MC, Dingkuhn M, Péré P, McNally KL, Luquet D. 2012. Developmental dynamics and early growth vigour in rice. I. Relationship between development rate (1/phyllochron) and growth. Journal of Agronomy and Crop Science **198**, 374–384.

Rebolledo MC, Luquet D, Courtois B, Henry A, Soulié J-C, Rouan L, Dingkuhn M. 2013. Can early vigour occur in combination with drought tolerance and efficient water use in rice genotypes? Functional Plant Biology **40**, 582–594.

Shi Z, Chang T-G, Chen F, *et al.* 2020. Morphological and physiological factors contributing to early vigor in the elite rice cultivar 9,311. Scientific Reports **10**, 14813.

Shipley B, Meziane D. 2002. The balanced-growth hypothesis and the allometry of leaf and root biomass allocation. Functional Ecology **16**, 326–331.

Shiraiwa T, Watatsu E, Horie T. 2006. Relative contribution of hetero- and auto-trophic growth to genotypic variation of seedling vigor in rice (*Oryza sativa* L.). Plant Production Science **9**, 133–140.

Skinner RH, Nelson CJ. 1995. Elongation of the grass leaf and its relationship to the phyllochron. Crop Science **35**, 4–10.

Tessmer OL, Jiao Y, Cruz JA, Kramer DM, Chen J. 2013. Functional approach to high-throughput plant growth analysis. BMC Systems Biology **7**, S17.

van den Boogaard R, Goubitz S, Veneklaas EJ, Lambers H. 1996. Carbon and nitrogen economy of four *Triticum aestivum* cultivars differing in relative growth rate and water use efficiency. Plant, Cell & Environment **19**, 998–1004.

Walker AP, Beckerman AP, Gu L, Kattge J, Cernusak LA, Domingues TF, Scales JC, Wohlfahrt G, Wullschleger SD, Woodward FI. 2014. The relationship of leaf photosynthetic traits–V cmax and J max–to leaf nitrogen, leaf phosphorus, and specific leaf area: a meta-analysis and modeling study. Ecology and Evolution **4**, 3218–3235.

Weraduwage SM, Chen J, Anozie FC, Morales A, Weise SE, Sharkey TD. 2015. The relationship between leaf area growth and biomass accumulation in *Arabidopsis thaliana*. Frontiers in Plant Science **6**, 167.

Xiong D, Liu X, Liu L, Douthe C, Li Y, Peng S, Huang J. 2015a. Rapid responses of mesophyll conductance to changes of CO_2 concentration, temperature and irradiance are affected by N supplements in rice. Plant, Cell & Environment **38**, 2541–2550.

Xiong D, Yu T, Liu X, Li Y, Peng S, Huang J. 2015b. Heterogeneity of photosynthesis within leaves is associated with alteration of leaf structural features and leaf N content per leaf area in rice. Functional Plant Biology **42**, 687–696.

Xiong D, Flexas J, Yu T, Peng S, Huang J. 2017. Leaf anatomy mediates coordination of leaf hydraulic conductance and mesophyll conductance to CO_2 in *Oryza*. New Phytologist **213**, 572–583.

Xiong D, Flexas J. 2018. Leaf economics spectrum in rice: leaf anatomical, biochemical, and physiological trait trade-offs. Journal of Experimental Botany **69**, 5599–5609.

Xiong D, Flexas J. 2021. Leaf anatomical characteristics are less important than leaf biochemical properties in determining photosynthesis responses to nitrogen top-dressing. Journal of Experimental Botany **72**, 5709–5720.

Xiong D. 2023. Leaf anatomy does not explain the large variability of mesophyll conductance across C_3 crop species. The Plant Journal **113**, 1035–1048.

Xiong D. 2024. Perspectives of improving rice photosynthesis for higher grain yield. Crop and Environment **3**, 123–137.

Yang G, Xiang H, Fu Y, Zhou C, Wang X, Yuan S, Yu X, Peng S. 2024. Optimal nitrogen management increases nitrogen use efficiency of direct-seeded double-season rice using ultrashort-duration cultivars. Field Crops Research **316**, 109495.

Yao X, Ata-Ul-Karim ST, Zhu Y, Tian Y, Liu X, Cao W. 2014. Development of critical nitrogen dilution curve in rice based on leaf dry matter. European Journal of Agronomy **55**, 20–28.

Zhang L, Richards RA, Condon AG, Liu DC, Rebetzke GJ. 2015. Recurrent selection for wider seedling leaves increases early biomass and leaf area in wheat (*Triticum aestivum* L.). Journal of Experimental Botany **66**, 1215–1226.

Zhao Z, Rebetzke GJ, Zheng B, Chapman SC, Wang E. 2019. Modelling impact of early vigour on wheat yield in dryland regions. Journal of Experimental Botany **70**, 2535–2548.